Review on various Methods used for Removal of Metal Artifacts from Dental Images

Shah Riddhiben, Biomedical Department, prof. Ghanshyam Parmar, Biomedical Department; Prof. J.B.Vyas
Biomedical Department
Government Engineering College, sec-28, Gandhinagar, India-382028

Abstract— This is a review paper showing different metal artifacts removal methods which are used mainly in X-ray CT. This method are mainly consists four stage procedure like filtered back projection, segmentation, Restoration and merging the segmented metallic object image with the filtered back-projection reconstructed image from the image. Many methods are presented for removal of metal artifacts like projection completion method, Filtered Back Projection (FBP) method, Maximum Likelihood TRansmission method (ML-TR), Iterative reconstruction method, Linear Interpolation (LI) method.

Index Terms- Filtered Back Projection (FBP) method, Iterative reconstruction method, Linear Interpolation (LI) method, Maximum Likelihood TRansmission method (ML-TR), Projection Completion Method.

I. INTRODUCTION

The main device in dental radiology is the X-ray projection image, which gives the structure of bone, soft tissues and Teeth. However, certain diagnostic and operative tasks often re-quire more precise knowledge of the three-dimensional (3-D) structure of oral tissues than is available in a single X-ray pro- jection image or a panoramic image [1, 2]. The artifact is a radial noise generated from the part of the metal when taking a CT image of a metalliferous verifiable object. [3]

In X-ray computed tomography (CT), the presence of strongly attenuating objects - such as dental fillings, surgical clips - causes typical streak artifacts in the reconstructed images (figure 1).[4]
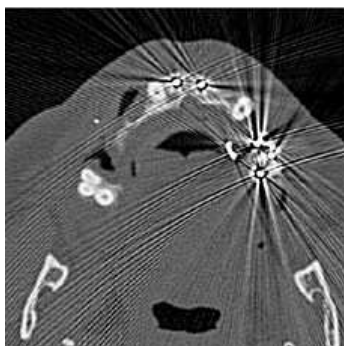

Figure 1: An example of metal streak artifacts in X-ray computed tomography.

According to B. De Man [5] main sources of metal artifacts are classify in four categories: Physics based which include beam hardening and under sampling artifacts, Patient based which include metallic and motion artifacts, Scanner based in which artifacts caused by detector sensitivity and mechanical instability (see in below table 1), Spiral based in which artifacts arise due to spiral interpolation [6, 7].
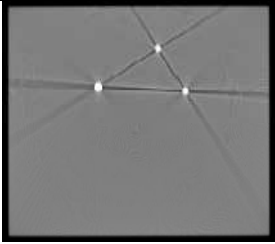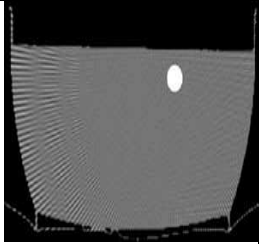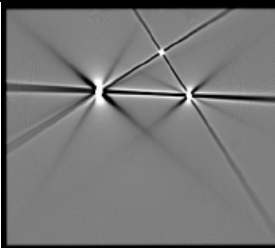

Table 1: Sources of metal artifacts in X-ray computed tomography.

In the following sections we describe the overview of various methods which are useful for reduce metal artifacts. In order to reduce the metal artifacts, there are some approaches [3] based on signal processing. Many algorithms are presented for reduction of metal streak artifacts in x-ray CT. Mainly those algorithm worked on reconstruction of projection data and segmentation of image in metallic and non-metallic objects and finally restoration technique which used for restore the image information by means of reduce the artifacts by using filtered back projection method for reconstruction [8], iterative reconstruction method [9], projection interpolation method [10]. For segmentation purpose they used thresholding technique [11].

The majority of MAR-methods consist of a modified reconstruction algorithm, in which metal objects are usually considered opaque and data corresponding to rays through the metal objects are defined as missing data.[10].Typically, MAR algorithms comprise two steps: a) metal trace identification, in which the projections corrupted by metallic implants are identified and b) artifact reduction, through which the identified missing projections are compensated for or treated in such a way that the associated streaking artifacts are mitigated.

Metal traces are conventionally identified by segmentation of metallic implants in FBP reconstructed images using thresholding [11] or clustering techniques [12], followed by reprojection of the obtained *metal-only* images onto the projection or sinogram domain. FBP is based on the assumption that every pixel can be characterized by a single parameter μ ,the linear attenuation coefficient, and that the logarithm of the measurement is the line integral of μ [8].

Other approaches are based on segmentation of metal traces directly in raw sinogram data using active contours [13], curve detection [14] and Markov random field (MRF) [10] techniques. The second step of MAR methods has been mainly explored by two classes of algorithms: projection completion and iterative image reconstruction.

Projected completion aims at interpolating the missing projections from their neighbors through linear, cubic spine and wavelet [15] interpolations or iterative in painting techniques using curvature-driven diffusion, total variation (TV) [13, 16], and wavelet regularization [17]. Bal and Spies proposed to replace the missing projections by the projections obtained from the forward projection of a tissue-classified CT image, namely tissue-class model or *prior* image. The problem with this approach is that the prior sinogram projections over missing regions (metal traces) are not well fitted with the projections of the original sinogram in immediate neighboring regions and hence, there is always a risk for discontinuities and generation of new artifacts. Recently, to solve this fitness problem, referred to as normalized MAR (NMAR), the original sinogram is normalized by the syndrome of prior image, thereby flattening neighboring projections. Then,

the missing data are linearly interpolated on the resulting sinogram is de-normalized. Projection completion has also been combined with algorithms that exploit the information hidden in low- and high-pass filtered sinograms [15] or low- and high-pass filtered reconstructed images. This class of algorithms is often fast and computationally appealing, however, if not efficiently implemented, these techniques might produce new artifacts. In fact, their efficiency depends on how robustly they can exploit the still available projection data even a prior knowledge in the recovery of missing data.

On the other hand, iterative reconstruction algorithms [9] establish another class of algorithms that, unlike FBP, attempt to frame the reconstruction problem in a way that more closely resembles reality. They can be adapted to missing data situations by down-weighting [8], ignoring the contribution of the corrupted projections, or can be tailored to polychromatic propagation models in order to reduce both beam hardening and metallic artifacts, [19]. However, this class of algorithms cannot entirely eradicate severe metallic artifacts; hence their initiation and combination [20] with projection completion techniques have also been investigated. But iterative image reconstruction techniques are still memory-demanding and computationally intensive. To reduce the computational complexity of this class of MAR algorithms, a region-based iterative reconstruction method in this fully polychromatic reconstruction model is used for metallic regions, while a simpler monochromatic model is used in other regions. It is worth noting that the model-based iterative algorithms have also been successfully applied for sinogram restoration and beam hardening correction.

II. METHODS

I. *Iterative reconstruction method*

We also apply iterative reconstruction [9] to reduce metal streak artifacts. The major advantage of this approach is the possibility to use a model of the acquisition, taking into account polychromaticity, scatter, noise, and any other imperfections. A general iterative reconstruction scheme is shown in figure 3.

In this method first we acquired image and calculated sinogram data. Then we compared this sinogram data with measured sinogram. If both are not matched those data are transformed in image domain further and corrected this. Now corrected image reconstructed again and again until calculated and measured data are not matched.
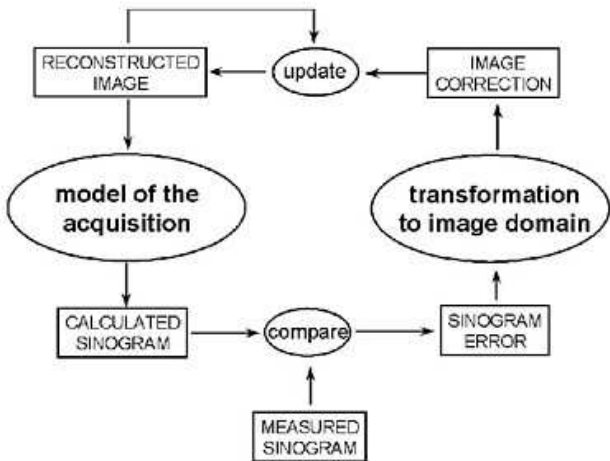
So disadvantage of this method is memory demanding for storage of all those data and time computation is very much.

II.   *Maximum Likelihood TRansmission method (ML-TR)*

Basic theory [8, 10]

For monochromatic acquisition model the basic idea is: given a set of transmission measurements $\{\mathcal{Y}_i\}_{i=1}^{I}$, find the distribution of linear attenuation coefficients $\{\mu_i\}_{j=1}^{J}$ that maximizes the log-likelihood (logarithm of the likelihood). [10]

$$\mathcal{L} = \sum_{i=1}^{I} (\mathcal{Y}_i \cdot \ln(\widehat{\mathcal{Y}_\iota}) - \widehat{\mathcal{Y}_\iota}) \dots\dots\dots\dots\dots (1)$$

Where $\widehat{\mathcal{Y}_\iota}$ is the expected number of photons detected along projection line i given the current reconstruction $\{\mu_i\}$. $\mathcal{Y}_i$ is assumed to be a Poisson realization of $\widehat{\mathcal{Y}_\iota}$. a simple acquisition model for transmission tomography is given by

$$\widehat{\mathcal{Y}_\iota} = b_i \exp\left(-\sum_{j=1}^{J} I_{ij}\mu_j\right) \dots\dots\dots\dots (2)$$

Where is the number of photons that would be detected in the absence of absorber (blank scan) and is the effective intersection length of projection line with pixel is measured by a calibration scan. In figure 4 we see simulated energy spectrum of intensity b_{ik}, where b_{ik} is total energy that would be detector by detector.

The algorithm is based on the transmission maximum-likelihood algorithm (ML-TR) [8, 10 and 21]. ML-TR reconstructs an attenuation image by optimizing the likelihood, assuming that the measured detector read-outs have a Poisson distribution.
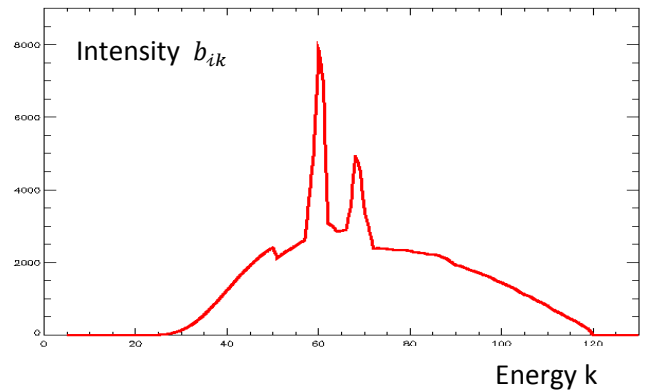
As a result, ML-TR attributes less weight to low-count detector read-outs, making the algorithm inherently robust against other sources of artifacts that are most prominent in directions of low counts, such as beam hardening, scatter, and partial volume effect.

In this method first take measured data and one blank sinogram data, compare both data and then update data is reconstructed using linear interpolation method. Finley reprojection of them is taken and this procedure is done until sufficient data is not get.

III.   *Iterative maximum likelihood polychromatic algorithm for ct(IMPACT) method*

For polychromatic acquisition model [8] basic idea is: a set of transmission measurements $\widehat{\mathcal{Y}_\iota}$ is given by

$$\widehat{\mathcal{Y}_\iota} = \sum_{k=1}^{K} b_{ik} \exp\left(-\sum_{j=1}^{J} I_{ij}\mu_{jk}\right) \dots\dots\dots\dots (3)$$

Where
k   energy index;
K   total number of energies;
μ_{jk} Linear attenuation coefficient in pixel j at energy k;
b_{ik} Total energy that would be detected by detector i absence of absorber for incident photons of energy E_k.

b_{ik} Is given[8] by using eq(4)

$$b_{ik} = I_{ik} \cdot S_k \cdot E_k \dots\dots\dots\dots (4)$$

Where
I_{ik} Emitted source spectrum (number of photons);
S_k Detector sensitivity (dimensionless);
E_k Photon energy (keV).

Two extensions of ML-TR method are introduced by B. De Man [10]. In this algorithm used Markov random

field for smoothness prior and then applies increased sampling in the reconstructed image.

1. A Markov random field smoothness, the reconstruction in parts of the image for which many high-count measurements are available, is mainly steered by the measured data, while the prior dominates in under-determined parts of the image. Markov random field smoothness prior is used with a Huber potential function which is given[10] by:

$$\emptyset(\mu) = \begin{cases} \dfrac{\mu^2}{2\delta^2} & \text{for } |\mu| \le \delta \\[2ex] \dfrac{|\mu| - \delta/2}{\delta} & \text{for } |\mu| \ge \delta, \end{cases} \quad \dots\dots\dots\dots (5)$$

Where δ is a positive constant. The Huber function is useful for edge-preserving purpose. The reconstruction in parts of the image, for which many high-count measurements are available, is mainly steered by the measured data, while the prior dominates in under-determined parts of the image.

2. Iterations are performed using a reconstruction image at double resolution. After the last iteration, the image is re-sampled to normal resolution. This higher resolution provides a better model for sharp transitions in the image.

This method is increased number of degrees of freedom which allows a better handling of other sources of artifacts, such as partial volume effect and beam hardening, and it makes the algorithm more robust.

IV.   *Projection completion method*

In projection interpolation based methods [10, 11], the projection data corresponding to rays through the metal objects is considered missing data. A prior art technique manually identified the missing projections and replaced them by interpolation of non-missing neighbour projections (as show in figure5).

MAR uses a polynomial interpolation technique to bridge the missing projections. Most metallic implants like joint replacements, osteosynthesis, dental implants, or surgical clips can be prevented by using this algorithm in scanner technology. In this method as shown in **figure 6 [11]**, first reconstructed using filtered back projection from original sinogram, then segmented by means of metal and project means non-metallic part then this projection is removed for sinogram.
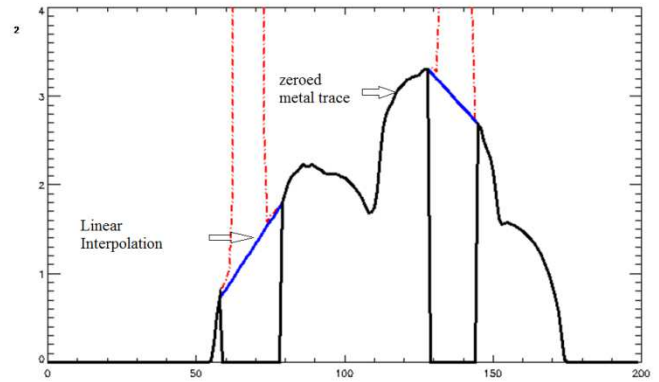

Figure 5: linear interpolation

Then using projection interpolation gets the projection for sinogram only non-metallic portion. Then finally we reconstructed this background projection and we get only metallic part after merging metal parts on it.
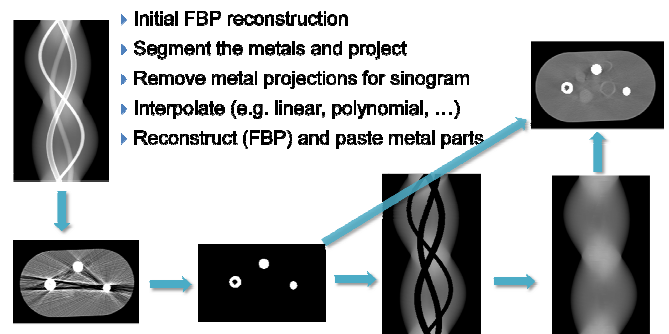

Figure 6: Process of projection completion method

So this method consists of following five steps [11]:

1. coarse image reconstruction,
2. metallic object segmentation,
3. forward-projection,
4. projection interpolation,
5. final image reconstruction.

The major innovations are 2-fold. First, a State-of-the-art mean-shift technique in the computer vision field is used to improve the accuracy of the metallic object segmentation. Second, a feedback strategy is developed in the interpolation step to adjust the interpolated value based on the prior knowledge that the interpolated values should not be larger than the original ones. Physical phantom and real patient datasets are studied to evaluate the efficacy of this method.

V.   *Compress sensing and sparsity driven method*

For a circular source trajectory, compressed sensing (CS) theory is presented by Jiyoung Choi, Min Woo Kim [22,23]. Compressed sensing theory allows aggressive view down sampling, which results in significant reduction of the overall computational time and burden of Iterative reconstruction process even without using any hardware acceleration. Even using angular down-sampling CS gives accurate reconstruction by exploit the

sparseness of metallic objects. And also this algorithm useful for imposes the consistency of the sinogram of data which are based on sparsity of metallic objects.

This algorithm is useful in many complicated scanner geometries like projection truncation in which small size detector is used compared to convention circular geometry. CS theory is applied for asymmetric placement of detector along the center [22].

Like convention CS application in this method whole jaw structure is not need. We assume non-metallic background is reconstructed separately which called residual sparse. As shown in figure7 [22,23] we first reconstructed residual image from original data which consists metallic parts and it define using **Eq. (6)** the sinogram $\widehat{p}_i$ and its noisy measurement p_i.

$$\widehat{p}_i = -\ln\frac{\lambda_i}{b_0} = \sum_{j=1}^{N} I_{ij}\mu_j \ \ and \ \ p_i = -\ln\frac{m_i}{b_0} \dots\dots\dots (6)$$

Where the total beam energy without attenuation is assumed as constant b_0. then an initial guess of metallic parts are segmented out from the FDK reconstruction using a simple threshold with a predefined value.

Using a ray tracing, we can then identify the locations of the sinogram that are corrupted by the metallic parts. The corrupted sinogram data are replaced with the linearly interpolated values from the surroundings, producing a metal removed sinogram. Suppose this interpolated sinogram as the corrected sinogram $\left\{\widehat{p}_i^{\ C}\right\}_{i=1}^{M}$. Then, the background voxel values $\{\mu_i\}_{i=1}^{N}$ are estimated using the corrected sinogram via the FDK algorithm [22,23].

As shown in figure7, finally using LI method, decomposition of unknown linear attenuation coefficients $\{\mu_i\}_{i=1}^{N}$ into background reconstruction $\{\mu_i^C\}_{i=1}^{N}$, and the residual images $\{\Delta\mu_i\}_{i=1}^{N}$, the following quantities are introduced:

$$\Delta p_i = p_i - \widehat{p}_i^{\ C} = -\ln\frac{m_i}{b_0} - \widehat{p}_i^{\ C} \dots\dots\dots (7)$$

$$\Delta\widehat{p}_i = \widehat{p}_i - \widehat{p}_i^{\ C} = -\ln\frac{\lambda_i}{b_0} - \widehat{p}_i^{\ C} = \sum_{j=1}^{N} I_{ij}\mu_j,$$
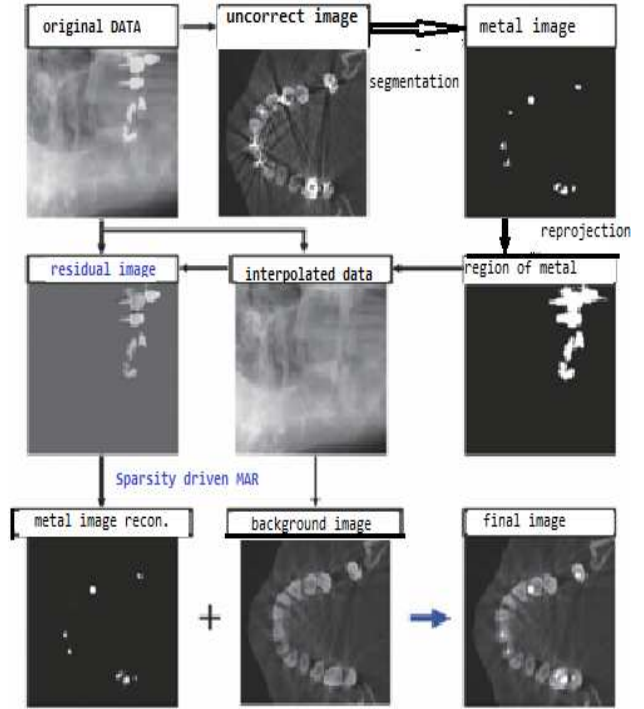$$i = 1, \dots, M, \qquad \dots\dots\dots (8)$$

Figure 7: schematic of sparsity-driven metallic artifact removal algorithm

In addition to the computational acceleration, CS-MAR algorithm has another important advantage. As described before, the whole objects are not always included within a FOV due to the limited detector size; however the metallic parts are usually contained within FOV, Iterative optimization methods can be applied without any problem.

III. RESULTS

1. ML-TR

Figure 8a shows the FBP reconstruction after projection completion using linear interpolation. Figure 8b shows the ML-EM reconstruction ignoring missing data. Figure 8c shows the ML-TR reconstruction ignoring missing data. Figure 8d repeats the reconstruction obtained with ML-TR at double resolution with Huber prior [8,10].
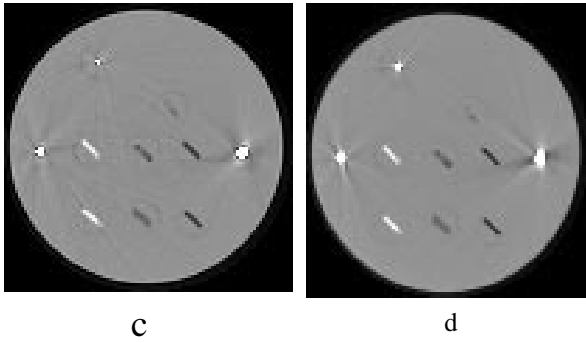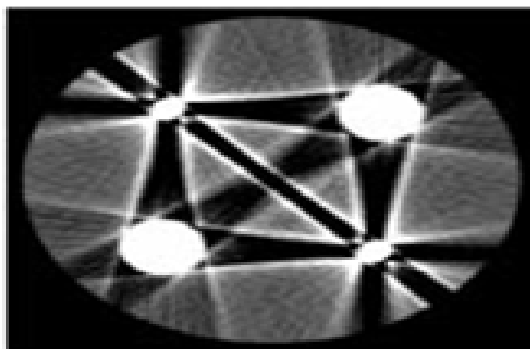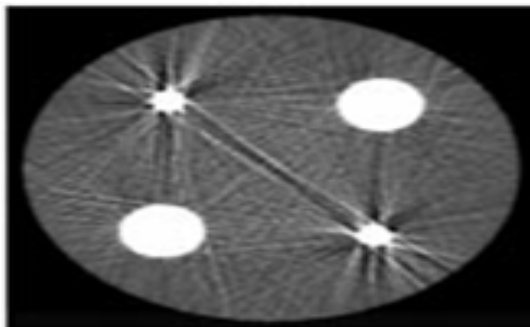

a   b
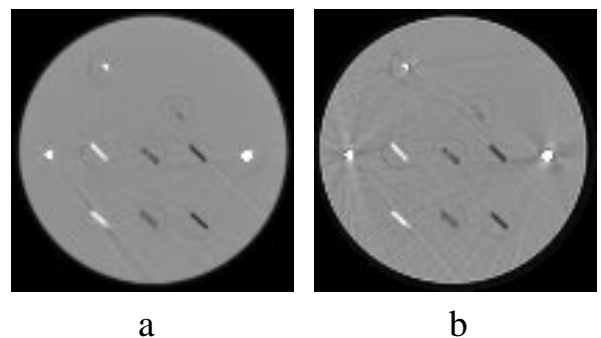
Figure 8: (a) FBP after projection completion. (b) ML-EM ignoring missing data. (c) ML-TR ignoring missing data. (d) ML-TR at double resolution with Huber prior.
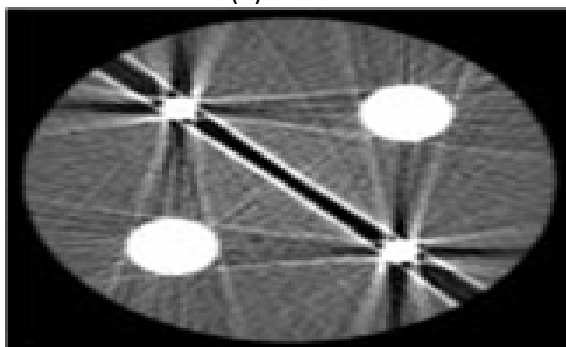
2. IMPACT

All measurement results are shown using a windowing interval $\mu =$[0.20; 0.24] cm which corresponds to a window of 200 HU and a level of 125 HU. The images are 20 cm ×20 cm and 256× 256 pixels [8].

(a) FBP

(b) IMPACT

(c) IBHC

Figure 9: Phantom (measurements). (a) FBP. (b) IMPACT. (c) IBHC.

Fig. 9 shows the reconstructions of phantom. The FBP reconstruction Fig. 9(a) exhibits severe streak artifacts. The dark streaks are reduced both with IMPACT Fig. 9(b) and IBHC Fig. 9(c). This indicates that the remaining streaks are mainly due to other effects, such as noise, scatter, the nonlinear partial volume effect, and aliasing. We can see the remaining dark streak in Fig. 9(c)— probably due to— scatter. This also suggests that IMPACT benefits from its correct noise model, which makes IMPACT robust against errors corresponding to strongly attenuated measurements.

3. CS-MAR

For physical experiments [22, 23], the projection data was measured using a clinical dental CT system (Picasso Trio, EWOO, Korea) that has width-truncated geometry.

3.1. Phantom Experiment Results

A physical phantom had been constructed with 10 metal nails fixed in a plate slightly tilted.
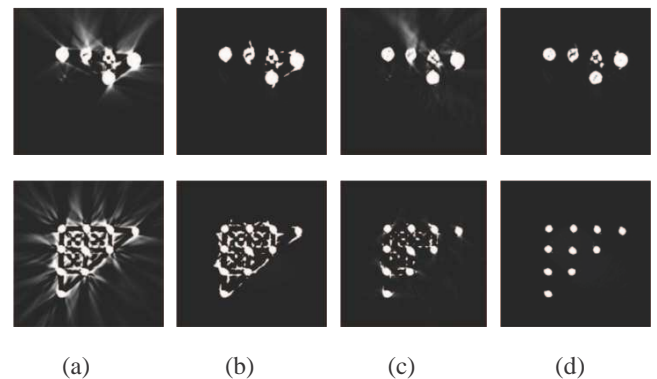

(a)　　(b)　　(c)　　(d)

Figure 10: Two different axial sections of reconstructed phantom are shown at top and bottom. Images are reconstructed by (a) FDK, (b) LI with a lower threshold (0.08), (c) LI with a higher threshold (0.12), and (d) CS-MAR using a threshold (0.08).

The WBP reconstruction in Figure 10(a) has severe streaking artifact especially between the metallic nails. The artifacts are not completely removed by LI as shown in Figure 10(b) and (c), whose thresholds values for metallic parts are differently set.

From the LI results in Figure 10(b) and (c), we have observed interesting trade-off between threshold and artifact removal in the LI approach. Although metallic insertion can be more clearly segmented with higher threshold, more severe metallic artifact still remains in background reconstruction. This is one of the fundamental limits of the LI approach.

However, CS-MAR is relatively free of such threshold dependent trade-off, since such spurious segmented noises can be effectively removed during FOCUSS update. Those spurious segmented parts from the low threshold value as used in Figure 10(b) can be effectively removed after six iterations of CS-MAR, as shown in Figure 10(d). Furthermore, even the inner structure of nails is visible in CS-MAR result.

3.2. In Vivo Results

Since various types of metal insertions can be located in one patient's jaw in in-vivo experiment, the threshold values for LI and CS-MAR were chosen in between the lowest intensity of metal insertion and anatomic structures.
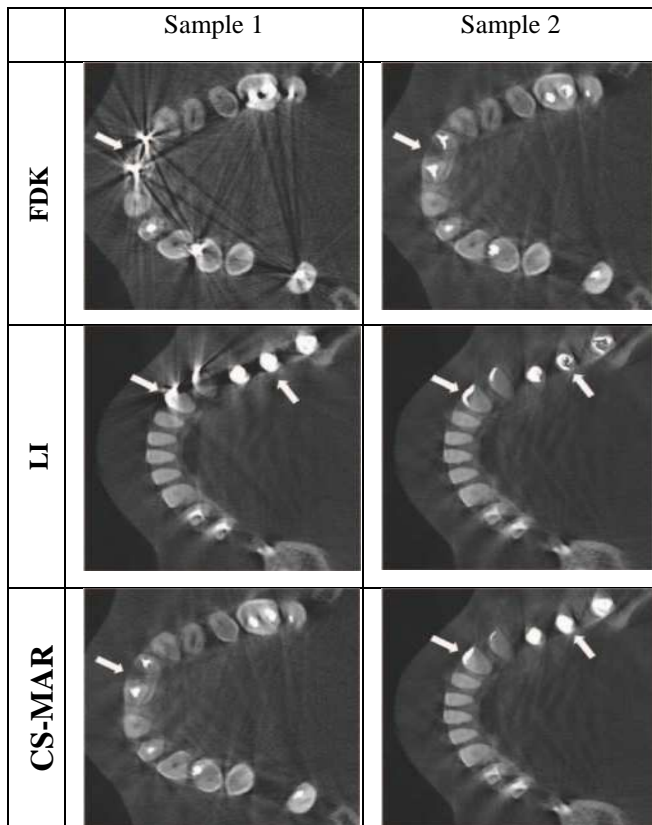
	Sample 1	Sample 2
FDK		
LI		
CS-MAR		

Table 2: **The axial sections of reconstruction from two different in vivo samples are shown above, respectively**. **Each image is reconstructed using (a) FDK, (b) LI, and (c) CS-MAR. For better comparison, images are magnified in jaw area. All the slices are shown at the same gray scale.**

In both of LI and CS-MAR, the streaking and shading artifacts laid in WBP are mostly gone so that we can verify the dental structure in arrowed region. Even though the background artifacts are removed, in LI result the metallic insertions have spurious shape since the metallic artifacts were included during the segmentation. On the other hand, CS-MAR can reconstruct dental fillings more realistically by removing the spurious artifacts. The CS-

MAR results, shown in table 2, were obtained using only 23 (25) views and after three FOCUSS iterations. Considering the size of volume data and the projection data, we can easily see the huge computational advantages of CS-MAR over the fully iterative methods.

IV. CONCLUSION

Our study indicates that ML-TR reconstruction using a-prior knowledge and using an increased number of degrees of freedom results in effective artifact reduction. Future work will attempt to improve the model of the scanner geometry, in order to reduce the remaining streaks. Additionally, we intend to study the use of explicit models for beam hardening, partial volume effect and scatter. This will allow reducing the weight of the prior, offering equally good artifact reduction with less smoothing. More complex phantoms with larger and more attenuating metal objects and with axial gradients must be studied. For application in clinical routine, a strong reduction of the computational cost of the algorithm is required.

We have also reviewed an iterative ML algorithm for CT (IMPACT) that prevents beam-hardening artifacts. Excellent results were obtained on phantom measurements. The algorithm has been compared to the post reconstruction approach, and the degree of beam-hardening correction was comparable for both algorithms. A strong reduction of computation time is required before being used routinely. Preliminary results indicate that metal artifact reduction is a very promising application for this new algorithm. Previous work has investigated the importance of the correct noise model. This paper addresses a second important cause of metal artifacts, namely beam hardening. Further research will extend the algorithm to include a prior, a model for scatter, and a model for the nonlinear partial volume effect.

Since the metallic objects usually occupy sparse support within a FOV, we can apply compressed sensing approach to MAR problem. The obtained l_1 penalized maximum likelihood criterion was implemented by a reweighted norm approach using FOCUSS. In phantom and in vivo experiments, the proposed CS-MAR outperformed FDK and LI in both restore the original shape of the metallic inserts as well as removing the shadow artifact that could lead to misdiagnosis. Furthermore, compressed sensing theory allows aggressive view down sampling, which results in significant reduction of the overall computational time of CS-MAR.

REFERENCES

1. Mehran Yazdi, and Luc Beaulieu, "A novel approach for reducing metal artifacts due to metallic dental implants" 2006 IEEE Nuclear Science Symposium Conference Record.

2. Abolfazl Mehranian, Mohammad Reza Ay, Member, IEEE , "3D Prior Image Constrained Projection Completion for X-ray CT Metal Artifact Reduction" IEEE Transactions On Nuclear Science, Vol. 60, No. 5, October 2013.

3. Keishi Mito, Hyoungseop Kim, Joo Kooi Tan, Seiji Ishikawa, Tatsuro Tanaka, Yasuhiro Morimoto "Method for Reduction of Metal Artifacts in Dental CT Images by Use of Frequency Analysis" International Conference on Control, Automation and Systems 2010.

4. Robert Manzke*, Michael Grass, and David Hawkes "Artifact Analysis and Reconstruction Improvement in Helical Cardiac Cone Beam CT"IEEE transactions on medical imaging, vol. 23, no. 9, september 2004.

5. B. De Man, J. Nuyts, P. Dupont, G. Marchal, and P. Suetens, "Metal streak artifacts in X-ray computed tomography: A simulation study," in Proc. IEEE Nuclear Science Symp. Conf. Rec., 1998, pp. 1860–1865.

6. B.De Man, J.Nuyts et al, "Metal Streak Artifacts in Xray Computed Tomography: A Simulation Study," IEEE Trans Nucl Sci, vol.46, nr.3, 1999, pp.691-696.

7. Mehran Yazdi, and Luc Beaulieu, "Artifacts in Spiral X-ray CT Scanners: Problems and Solutions" International Journal of Biological and Life Sciences 43:2008.

8. B. De Man, J. Nuyts, P. Dupont, G. Marchal, and P. Suetens, "An iterative maximum-likelihood polychromatic algorithm for CT," IEEE Trans. Med. Imag., vol. 20, no. 10, pp. 999–1008, Oct. 2001.

9. Benoit Hamelin, Yves Goussard, David Gendron, Jean-Pierre Dussault, "Iterative ct reconstruction of real data with metal artifact reduction" International Journal of Biological and Life Sciences 2008, 978-1-4244-2003-2/08/$25.00 ©2008 IEEE.

10. B. De Man, J. Nuyts, P. Dupont, G. Marchal, and P. Suetens, "Reduction of metal streak artifacts in X-ray computed tomography using a transmission maximum a posteriori algorithm," IEEE Trans. Nucl. Sci., vol. 47, no. 3, pp. 977–981, Jun. 2000.

11. Hengyong Yu, "Technical report on A Segmentation-Based Method for Metal Artifact Reduction"AUR,2007doi:10.1016/j.acra.2006.12.015.

12. Yizong Cheng, "Mean Shift, Mode Seeking, and Clustering" in IEEE transactions on pattern analysis and machine intelligence, vol. 17, no. 8, august 1995.

13. H. Xue, L. Zhang, Y. Xiao, Z. Chen, and Y. Xing, "Metal artifact reduction in dual energy CT by sinogram segmentation based on active contour model and TV inpainting," in Proc. IEEE Nuclear Science Symp. Conf. Rec., 2009, pp. 904–908.

14. C.Xu,F.Verhaegen,D.Laurendeau,S.A.Enger,andL.Beaulieu, "An algorithm for efficient metal artifact reductions in permanent seed implants," Med. Phys., vol. 38, no. 1, pp. 47–56, 2011.

15. S. Zhao, D. Robertson, G. Wang, and B. Whiting, "X-ray CT metal artifact reduction using wavelets: An application for imaging total hip prostheses," IEEE Trans. Med. Imag. , vol. 19, pt. 12, pp. 1238–1247, Dec. 2000.

16. X. Duan, L. Zhang, Y. Xiao, J. Cheng, Z. Chen, and Y. Xing, "Metal artifact reduction in CT images by sinogram TV inpainting," in Proc. IEEE Nuclear Science Symp. Conf. Rec., 2008, pp. 4175–4177.

17. A. Mehranian, M. R. Ay, A. Rahmim, and H. Zaidi, "X-ray CT metal artifact reduction using wavelet domain sparse regularization," IEEE Trans Med Imag.,tobepublished.

18. K. Y. Jeong and J. B. Ra, "Metal artifact reduction based on sinogram correction in CT," in Proc. IEEE Nuclear Science Symp. Conf. Rec., 2009, pp. 3480–3483.

19. J. Nuyts and S. Stroobants, "Reduction of attenuation correction artifacts in PET-CT," in Proc. IEEE Nuclear Science Symp. Conf. Rec., 2005, pp. 1895–1899.

20. C. Lemmens, D. Faul, and J. Nuyts, "Suppression of metal artifacts in CT using a reconstruction procedure that combines MAP and projection completion," IEEETrans.Med.Imag., vol. 28, no. 2, pp. 250–260, Feb. 2009.

21. J. La Riviere, J. Bian, and P. A. Vargas, "Penalized-likelihood sinogram restoration for computed tomography," IEEE Trans. Med. Imag., vol. 25, no. 8, pp. 1022–1036, Aug. 2006.

22. Jiyoung Choi , Min Woo Kim , Won Seong , and Jong Chul Ye," Compressed sensing metal artifact removal in dental ct" International conference of image processing and biomedical imaging 2009, 978-1-4244-3932-4/09/$25.00 ©2009 IEEE.

23. Jiyoung Choi , Min Woo Kim , Won Seong , and Jong Chul Ye, "Sparsity driven metal part reconstruction for artifact removal in dental CT" Journal of X-Ray Science and Technology 19 (2011) 457–475 DOI 10.3233/XST-2011-0307 IOS Press.